ELSEVIER

Radiotherapy and Oncology 60 (2001) 181–190

RADIOTHERAPY & ONCOLOGY
JOURNAL OF THE EUROPEAN SOCIETY FOR THERAPEUTIC RADIOLOGY AND ONCOLOGY

www.elsevier.com/locate/radonline

Pre-treatment dosimetric verification by means of a liquid-filled electronic portal imaging device during dynamic delivery of intensity modulated treatment fields

Ann Van Esch*, Bianca Vanstraelen, Jan Verstraete, Gerald Kutcher, Dominque Huyskens

Department of Oncology, Division Radiation Physics, University Hospital Gasthuisberg, Herestraat 49, B-3000 Leuven, Belgium

Received 31 July 2000; received in revised form 12 December 2000; accepted 9 January 2001

Abstract

Background and purpose: Although intensity modulated radiation therapy is characterized by three-dimensional dose distributions which are often superior to those obtained with conventional treatment plans, its routine clinical implementation is partially held back by the complexity of the beam verification. This is even more so when a dynamic multileaf collimator (dMLC) is used instead of a segmented beam delivery. We have therefore investigated the possibility of using a commercially available, liquid-filled electronic portal imaging device (EPID) for the pre-treatment quality assurance of dynamically delivered dose distributions.

Methods and materials: A special acquisition mode was developed to optimize the image acquisition speed for dosimetry with the liquid-filled EPID. We investigated the accuracy of this mode for 6 and 18 MV photon beams through comparison with film and ion chamber measurements. The impact of leaf speed and pulse rate fluctuations was quantified by means of dMLC plans especially designed for this purpose. Other factors influencing the accuracy of the dosimetry (e.g. the need for build-up, remanence of the ion concentration in the liquid and bulging of the liquid at non-zero gantry angles) were studied as well. We finally compared dosimetric EPID images with the corresponding image prediction delivered without a patient in the beam.

Results: The dosimetric accuracy of the measured dose distribution is ~2% with respect to film and ion chamber measurements. The accuracy declines when leaf speed is increased beyond 2 cm/s, but is fairly insensitive to accelerator pulse rate fluctuations. The memory effect is found to be of no clinical relevance. When comparing the acquired and expected distributions, an overall agreement of 3% can be obtained, except at areas of steep dose gradients where slight positional shifts are translated into large errors.

Conclusions: Accurate dosimetric images of intensity modulated beam profiles delivered with a dMLC can be obtained with a commercially available, liquid-filled EPID. The developed acquisition mode is especially suited for fast and accurate pre-treatment verification of the intensity modulated fields.

Keywords: Dynamic multileaf collimator; Dosimetric verification; Liquid-filled electronic portal imaging device

1. Introduction

The implementation of intensity modulated beams into the clinical routine of radiotherapy can offer substantial advantages to the patient regarding dose distribution in the target volume accompanied by improved sparing of the surrounding normal tissue and critical organs (see [2,10]). One technique for the delivery of intensity modulated beams is the sliding window technique with a dynamic multileaf collimator (dMLC). Although this technique offers many advantages in comparison with the step and shoot technique, its verification is more complex due to its dynamic nature. The dosimetric accuracy and reproducibility of the dMLC can be verified using films in a phantom [2,7,17]: prior to the first treatment session, all intensity modulated fields are transferred from the patient treatment plan to a flat polystyrene phantom; dose distributions calculated by the treatment planning system (TPS) are then compared with the dose distributions measured with film. Apart from the fact that this is a time consuming procedure, it contains all the disadvantages inherent to film dosimetry, such as the limited dosimetric range and the necessity for a sensitometric curve to convert optical density to dose. Electronic portal imaging devices (EPIDs) offer the advantage that they provide on-line, digital images and would therefore be the ideal tool for verification. When referring to EPID verification, one can make a distinction between leaf positioning verification (e.g. [6]) and dosimetric verification. Ma et al.

* Corresponding author.

0167-8140/01/$ - see front matter
PII: S0167-8140(01)00305-X

[9] employed a fast beam imaging system (BIS, Wellhöfer, Germany) and compared measured images with reference images generated from the MLC leaf sequencing files. Gross errors, such as flipped reference images, are readily detected by the presented procedure, but positional errors of 0.5 mm in the leaf motion could also be intercepted. Curtin-Savard et al. [4] reported on the use of a liquid-filled portal imager for the dosimetric verification of step-and-shoot delivery by acquiring a portal image for every subfield of the leaf sequence. Subsequent to their calibration, the images were multiplied by their respective associated monitor unit (MU) settings, and summed to produce a planar distribution at the measurement depth in a phantom. These distributions were then compared with dose distributions predicted by the TPS. A drawback of their method is the above mentioned need for MU settings as well as the time required per treatment field: for the acquisition and postprocessing of one typical clinical field, a total time of 1 h is needed [4]. Pasma et al. [12] reported on the use of a CCD-camera based fluoroscopic EPID for pre-treatment verification of intensity modulated beams produced with a dMLC. Due to the high data acquisition rate of these cameras and their capability to measure simultaneously in all points of the treatment field, integrated images could be obtained, these images were then converted into two-dimensional dose distributions and compared with the calculated dose distributions. The time required to obtain a dosimetric image of an intensity modulated field is about 2 min. For the reported profiles, the agreement between calculations and EPID measurements was within 2% (1 SD). Chang et al. [3] developed a quality assurance procedure to assess the intensity profile and dosimetry for intensity modulated treatments fields using a liquid-filled portal imaging device (PortalVision Mk1, Varian Medical Systems, Palo Alto, CA). To overcome the limited acquisition rate of their detector (5 s/image for the fast acquisition mode), the leaf speed was intentionally slowed down by drastically (e.g. ten-fold) increasing the amount of MUs. Apart from the fact that this inevitably increases the treatment verification time, any error influenced by the speed of the leaves is missed and verification is not complete. It also renders the method inapplicable for verification during the actual treatment.

We have investigated the use of a commercially available, liquid-filled EPID (PortalVision Mk2, Varian Medical Systems) for dosimetric verification of intensity modulated beam profiles, delivered with a dynamic MLC. Rather than artificially decreasing the leaf speed, however, a special, fast mode was developed in cooperation with the manufacturer (Varian Medical Systems) to optimize the acquisition speed and to render the EPID operational for routine dosimetric verification of clinical intensity modulated fields prior to treatment initiation, and eventually, also during the actual treatment. We have studied the accuracy of the developed dosimetric acquisition mode as well as its limitations, and we have compared the obtained dosimetric images with the image predictions.

2. Materials and methods

2.1. EPID hardware and software

The EPID used in our study is a commercially available, liquid-filled portal imaging device (PortalVision Mk2, Varian Medical Systems), mounted on a Clinac 2100 C/D with dynamic MLC (80 leaves; Varian Medical Systems). This system includes: (i), an image detection unit (IDU) featuring the detector and accessory electronics; (ii), an image acquisition unit (IAS2) containing the drive and acquisition electronics and interfacing hardware; and (iii), a dedicated workstation (PortalVision PC) located outside the treatment room. The IDU is essentially a matrix of 256×256 straight wire electrodes enclosing an 0.8 mm thick layer of isooctane, producing a matrix of miniature ion chambers with a pixel size of 1.27×1.27 mm^2 and a total sensitive area of 32.5×32.5 cm^2. The construction materials in front of the liquid film (upper electrode plate, build-up and upper stabilizing plate) have a water-equivalent thickness of 8 mm, as specified by the manufacturer. The IAS2 controls and reads the image detector. Its local hard disk contains the image correction images and acquisition parameters. The time required for one electrometer read out is typically 6.5 μs, adding up to a minimum of 0.9 ms for one row of ion chambers. The rest of the row cycle time is the time between switching the high voltage and starting the readout (typically 1 ms) and signal processing time. The ionization of the liquid film is measured by applying high polarizing voltage pulses (400 V), one row at a time. The parameters that determine the acquisition time for one frame are the height and length of polarizing high voltage pulses and the amount of times a single row is scanned for averaging purposes. Typical image acquisition modes used in clinical routines have image scan times of about 2.5–5 s. In the acquisition mode used for our study, however, high voltage pulses of 400 V were limited to 2.0 ms and the frame acquisition time was reduced to a minimum (i.e. a scan time of 0.7 s for a full resolution image).

2.2. Dose–response relationship

The conversion of measured pixel values into dose rates involves several operations. We assume that an uncorrected pixel value at the location of pixel (ij) in the detector is related to the local dose rate according to Eq. (1)

$$r_{ij} = s_{ij} \cdot G\left(\dot{D}_{ij}\right) + o_{ij} + E_i \quad (1)$$

where r_{ij} denotes the pixel value in a raw frame, s_{ij} the relative sensitivity or gain, o_{ij} the offset of each individual ion chamber, E_i the offset attributed to each electrometer, $\dot{D}_{ij}$ the local dose rate, and G the absolute dose response of the detector. The electrometer offsets are measured without polarizing voltage prior to the acquisition of each frame, and immediately subtracted in the acquisition system. The pixel offsets, o_{ij}, are obtained by acquiring a dark field image, i.e. an image

without radiation. The differences in individual chamber sensitivity are measured in a large photon field, the so-called flat field, covering the whole area of the detector. These dark and flat field corrections are performed every 2 months. Correction parameters are downloaded to the image acquisition system (IAS2), and for routine imaging, raw pixel values are immediately converted before being transferred to the external workstation.

The dose–response relationship for a liquid-filled EPID has been reported in the literature for static field delivery [1,5]. Essers et al. describe the relation between the ionization current and dose rate by an equation (Eq. (2)) with two terms: one main term proportional to the square root of the dose rate and one correction term linear to the dose rate

$$G(\dot{D}) = a\dot{D}^{1/2} + b\dot{D} \quad (2)$$

The weight factors, a and b, depend on the photon beam energy, pulse rate frequency and image acquisition mode. Therefore, they have to be determined for each EPID and accelerator setting separately. For imaging or dosimetry of static field delivery, data acquisition on the portal imager is synchronized to the accelerator pulse pattern and a linear correction algorithm approaches the ion recombination in the detector in between accelerator pulses.

2.2.1. Dose–response relationship in dynamic mode

Although fast data acquisition is advantageous for imaging as well, it is of even more importance in dynamic dosimetry for two reasons. Obviously, frame acquisition should be fast compared with the leaf movement. Secondly, during the delivery of intensity modulated dMLC beams, pulse rate fluctuations are often unavoidable in order to assure correct correspondence between actual leaf position and delivered MU. As a consequence, the time between two accelerator pulses is no longer constant and some of the assumptions in the mathematical derivation [1] of Eq. (2) break down. Therefore, the acquisition mode developed for dosimetric verification of dMLC fields aims to determine the average ion concentration physically, through fast data acquisition rather than through synchronization on the accelerator pulses.

Instead of Eq. (2), a power law description of the dose–response relationship was used [15], since the latter provides a qualitatively equivalent description of the dose–response relationship while offering some mathematical and practical advantages over the former

$$G(\dot{D}) = \alpha\dot{D}^{\beta} \quad (3)$$

In correspondence to Eq. (2), β is slightly larger than 0.5 and α is always positive. One practical advantage of this dose–response relationship is that, in contrast to Eq. (2), it allows the gain correction to be moved out of the frame averaging loop, as can be seen from inserting Eq. (3) into Eq. (1). Individual frames are only corrected for the dark field offset and then converted to dose rate at the IAS2 acquisition Central Processing Unit (CPU) (by means of a look-up table based upon the calibration parameters, and downloaded to the IAS2). A pixel-wise multiplicative flat field correction is applied after adding up the individual dose rate frames. This both accelerates the acquisition and facilitates the handling, as the latter can be implemented on the external PortalVision PC rather than on the IAS2 acquisition CPU.

By multiplying the averaged dose rate (i.e. the sum of all individual dose rate frames divided by the total number of frames) with the total acquisition time, we finally obtain the absolute dose.

The calibration of α and β of the dMLC acquisition mode was performed for 6 and 18 MV beams; the pulse rate frequency was set at 300 MU/min (i.e. the standard dose rate setting for the delivery of IMRT fields at our department) and synchronization to the accelerator pulse pattern was switched off. Calibration was performed with a polystyrene slab of 2 cm thickness placed on top of the portal imager housing. Although we will refer to the latter as build-up material, this polystyrene slab primarily serves as a filter to eliminate scattered electron contamination rather than to measure at a depth of maximum build-up, since the construction of the detector is such that a 6.6 cm airgap remains between the detector cover and the liquid imaging plane. The actual calibration procedure is divided into a relative (β) and absolute (α) part: both parameters are calculated from measurements in the central region of the detector. β is determined by acquiring open beam images ($15 \times 15\ cm^2$) at different focus detector distances (FDD) and assuming an inverse square law relationship between dose rate and FDD. Subsequently, α is calculated from correlating one EPID measurement to one ion chamber measurement, with the ion chamber positioned (below 2.8 cm build-up) at the same distance as the EPID detector plane.

2.3. Build-up requirements

The need for build-up material on the EPID surface to avoid or minimize the contribution of scattered electrons to the measured dose rate was investigated by ion chamber measurements (PTW-Freiburg, Germany, type 61002, $0.125\ cm^3$). The ion chamber was placed on the beam-axis behind a 20 cm thick polystyrene, rectangular phantom (positioned at a fixed SSD of 80 cm) in a mini-phantom ($7 \times 7\ cm^2$). The dose rate was measured at several distances between the exit surface of the phantom and the ion chamber, ranging from 9 to 75.5 cm (Fig. 1). Measurements were performed with an 18 MV beam ($10 \times 10\ cm^2$, 600 MU), and the build-up on the ion chamber was varied from 0.8 to 6.6 cm.

The aim was to determine the minimum required build-up in order to eliminate, or at least minimize, the contribution from scattered electrons.

While build-up material may be a necessity for accurate dosimetry, the image quality for patient positioning purposes may deteriorate significantly were this build-up material permanently mounted into the portal imager. By

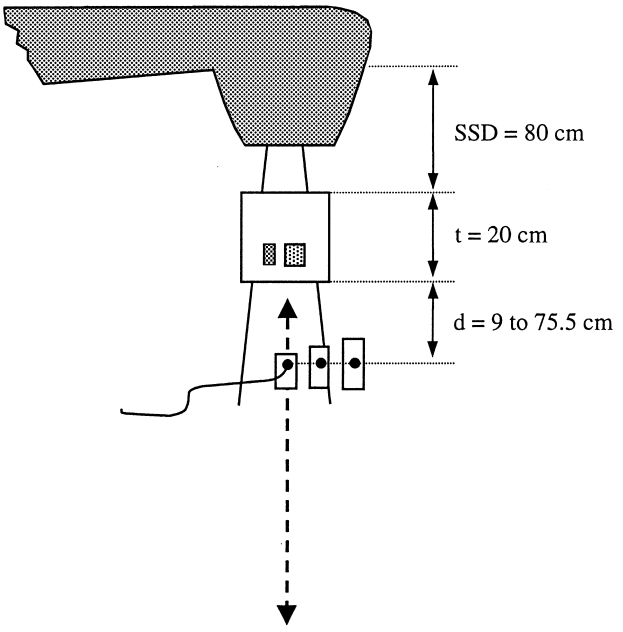

Fig. 1. Schematic view of the measurement set-up for on-axis ion chamber measurements in a mini-phantom at several distances (*d*) behind a 20 cm thick polystyrene multipurpose phantom. Measurements were performed with an 18 MV beam (field size, 10×10 cm^2) Build-up on the ion chamber was varied from 0.8 to 6.6 cm.

means of a Las Vegas phantom, we have therefore evaluated the changes in contrast and resolution induced by the build-up for 6 and 18 MV, for different thicknesses of polystyrene (1 and 2 cm), as well as for 1 mm copper.

2.4. Accuracy assessment of the EPID in dynamic mode

2.4.1. Relative dosimetry

The relative dosimetric accuracy was assessed by means of intensity modulated fields with a stepwise dose profile, generated through the inverse treatment planning module of the Cadplan TPS (Varian Medical Systems) on a polystyrene rectangular phantom in which three adjacent rectangular target volumes were defined, each with a different dose prescription. Unless stated otherwise, all dosimetric EPID images were obtained with a 2 cm polystyrene slab placed on the detector housing. Dosimetric EPID images were compared with film measurements (ready pack Kodak X-Omat V for therapy verification), performed with 2.8 cm polystyrene build-up and ion chamber measurements in a water phantom at a depth of 2.8 cm (since 2.8 cm is also the total amount of build-up on the EPID). Both film and ion chamber measurements were performed in the plane of the detector. Each data point in the latter dose profile was acquired by delivering the whole dynamic field at every ion chamber position (in steps of 5 mm).

2.4.2. Data acquisition speed versus leaf speed

To assess the limitations of the dosimetric acquisition mode regarding data acquisition speed versus leaf speed, individual blocks of four pairs of opposed leaves were programmed to move at different, but constant speeds, retaining a gap of 1 cm. The total amount of delivered MU was chosen to be 75 MU, so that the fastest leaf block moved at maximum leaf speed (i.e. 3 cm/s), but without causing a decrease in the accelerator pulse repetition rate. The resulting stepwise profiles were compared relatively with film and EPID dosimetric images. The film was irradiated by four-fold delivery of the dynamic treatment with 75 MU to obtain the optimum optical density. The EPID reference image was acquired by delivering a higher total number of MU (400 MU) to assure sufficiently fast data acquisition compared with leaf speed.

2.4.3. Absolute dosimetry

To evaluate the use of the liquid-filled portal imager as a tool for absolute dosimetry, the short- and long-term absolute reproducibility of the dosimetric images was verified by comparing several dosimetric images of the same dynamic delivery, for 6 and 18 MV photon beams, acquired on the same day and over a span of several weeks, respectively. The linearity of the integrated dose as a function of the total amount of MUs was studied by comparing dosimetric images of the same dynamic MLC plan (e.g. the stepwise profile used for relative dosimetric accuracy), but delivered with different multiples of 100 MU.

2.4.4. Calibration versus accelerator pulse rate frequency

Since a pulse rate frequency of 300 MU/min is used for the calibration of α and β (cf. Eq. (3)), the generality of these calibration values was checked because pulse rate fluctuations are often inherent to dynamic delivery. Firstly, calibrations were also performed for dose rate settings of 100 and 200 MU/min. These calibrations were performed with the dark and flat field corrections of the 300 MU/min mode and identical acquisition parameter settings; the resulting values for α and β were compared with the ones obtained with 300 MU/min. Subsequently, dosimetric images of the same dynamic delivery and converted by means of the 300 MU/min calibration parameters, but with different actual dose rates were compared. Thirdly, rather than obtaining dosimetric data during delivery with a different, but still constant, pulse repetition frequency, pulse rate fluctuations were artificially induced within one dynamic field delivery by creating otherwise identical dMLC plans with different leaf tolerance settings (0.05 versus 0.2 mm). Although the dosimetric accuracy of the delivery is the same for both tolerance settings (this was double-checked with film measurements), a very low tolerance on leaf position causes an irregular pulse pattern.

2.4.5. Memory effect of the EPID

Liquid-filled EPIDs are known to exhibit a memory effect [4,5,16]. Essers et al. [5] reported a change in sensitivity due to short-term irradiation damage, with a time constant of several minutes. We have studied the memory effect

connected to the ion lifetime. The theoretical decay of the ion concentration $n(t)$ in the liquid-filled ion chambers as a function of time after irradiation is described by the differential equation,

$$\frac{dn(t)}{dt} = -\nu n(t)^2 \tag{4}$$

where the recombination constant, ν, has a value of 1.5×10^{-16} $m^3 s^{-1}$ [16]. Solving this equation yields

$$n(t) = \left(\nu t + \sqrt{\frac{\nu}{n_{t=0}}}\right)^{-1} \tag{5}$$

This decay was experimentally monitored by fast acquisition of a series of images after the beam was switched off. To assess the implications on dosimetry in the clinical routine, a separate test was performed: 1000 MU were delivered to the portal imager in a 5×5 cm^2 static field, immediately followed by delivery of 20 MU in a 15×15 cm^2 static field, during which a dosimetric image was acquired.

2.4.6. Image acquisition versus gantry angle

At non-zero detector angles, the pressure distribution in the liquid is not uniform due to gravity, causing local sensitivity changes of a few percent. This so-called bulging effect is noticeable as a gradient in the lateral images. We assessed the possibility and accuracy of implementing a correction algorithm. The applied correction at gantry angle, γ, is based upon the use of a standard dark field correction and an angle dependent flat field correction $FF(\gamma)$. The flat field correction array for a given angle contains an average and a differential term weighted with the influence of gravity,

$$FF(\gamma) = \frac{FF_{cal}(0°) + FF_{cal}(90°) + FF_{cal}(180°) + FF_{cal}(270°)}{4} + \sin(\gamma) \cdot \frac{FF_{cal}(90°) - FF_{cal}(270°)}{2} \tag{6}$$

i.e. $FF(\gamma)$ is obtained from calibration images FF_{cal} acquired at gantry angles 0, 90, 180 and 270°. To retain the high frame acquisition speed, the flat field correction for the dynamic delivery mode is again applied on the final, integrated image, i.e. the correction algorithm is implemented at the level of the PortalVision workstation rather than at the IAS2.

Open field images covering the entire sensitivity area of the detector were obtained for a full gantry rotation (in steps of 10°) to evaluate the accuracy of the correction algorithm as a function of gantry angle. The flatness of these test images was quantified, with and without applying the correction algorithm, by calculating the SD from the expected value over the whole detector area (except for a small margin of 4 pixels at the edges).

2.5. Portal dose image prediction

A dosimetric image of an intensity modulated treatment delivery can only be properly evaluated if an accurate prediction of the image can be calculated. We have evaluated the portal dose image prediction algorithm developed by Pasma et al. for portal dose measurements using a fluoroscopic EPID [11]. The calculation modules are linked to the Cadplan TPS as research software and use the expected beam fluence matrix as determined in the treatment planning process as a starting point. For each beam quality, the required input data for dosimetric image prediction are derived from a limited number of measured beam data. The calculation of the portal dose at the plane of the detector in the absence of a patient is based on the algorithm developed by Storchi et al. [13,14], using pencil beam kernels. With a patient in the beam, patient anatomy as described by the planning CT-scan is taken into account and the portal dose is described by the image without the patient multiplied by a transmission function. The contributions from primary and scattered photons (generated through interaction with the patient) to the transmission function are calculated separately and subsequently added. The algorithms for the calculation of this function are based on data derived from measured transmissions through flat, water-equivalent (polystyrene) phantoms. To be able to use these data for the derivation of the transmission through an inevitably inhomogeneous patient, the anatomy as described by the CT-data is substituted by an (imaginary) equivalent homogenous phantom consisting of polystyrene [11]. For each ray line, the patient and the equivalent homogeneous phantom have equivalent polystyrene thicknesses and equal distances between the center of mass and the detector plane.

We have evaluated the method for our liquid-filled ion chamber EPID at a fixed FDD of 145 cm (as used in clinical routine). With pre-treatment verification as our main goal, the emphasis was on predictions without a phantom in the photon beam. For stepwise profiles as well as for some intensity modulated prostate fields, expected images were calculated and compared with the accordingly acquired dosimetric EPID images. All EPID data were obtained at zero gantry angle.

Since eventually, the EPID may prove a useful tool for dosimetric verification during treatment as well, we did some preliminary tests on image prediction taking the presence of a phantom into account. The phantom used for this evaluation was the rectangular multipurpose polystyrene phantom containing heterogeneities (cork and air) as depicted in Fig. 1, rather than the Alderson pelvis phantom because of the unavoidable, and difficult to reproduce, airgaps in between the different slices of our humanoid phantom.

3. Results

3.1. Dose–response relationship

3.1.1. Dose–response relationship in dynamic mode

The dose–response relationship as measured and fitted for

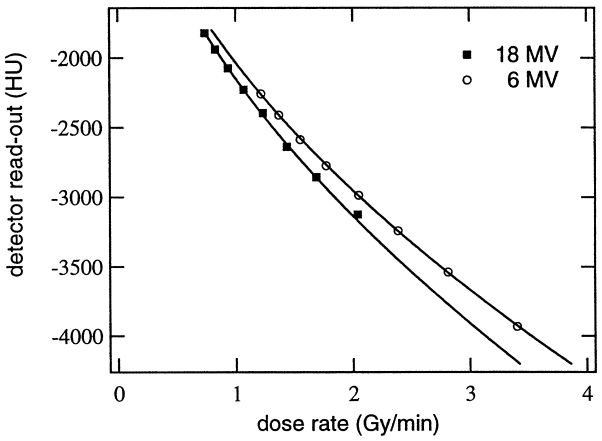

Fig. 2. Dose rate–response relationship as measured and fitted for 6 and 18 MV beams. The detector response is measured in Houndsfield units (HU).

6 and 18 MV photon beams is shown in Fig. 2. The fit values for α and β were -2033 and 0.5369 for 6 MV, and -2148 and 0.5447 for 18 MV. The maximum and average fitting errors with respect to the mean calculated dose rate value were 0.4 and 0.3% for 6 MV, and 0.7 and 0.3% for 18 MV, respectively.

3.2. Build-up requirements

Fig. 3 presents the ion chamber measurements in a mini-phantom under different build-up conditions as a function of airgap between phantom and detector surface. All curves were normalized to their measuring point at largest airgap (i.e. 75.5 cm). Relative behavior as a function of airgap becomes comparable for build-up material beyond 2.8 cm: at a clinically relevant airgap of 20 cm, the slopes agree within 3% (-0.0480 ± 0.0014 cm^{-1}). However, in cases of 0.8 and 1.6 cm build-up, at the same distance behind the exit surface, slopes of 0.064 and 0.097 were measured, respectively. Hence, differences up to 4.6%/cm airgap will occur between relative dose profiles measured with 0.8 versus 2.8 cm build-up.

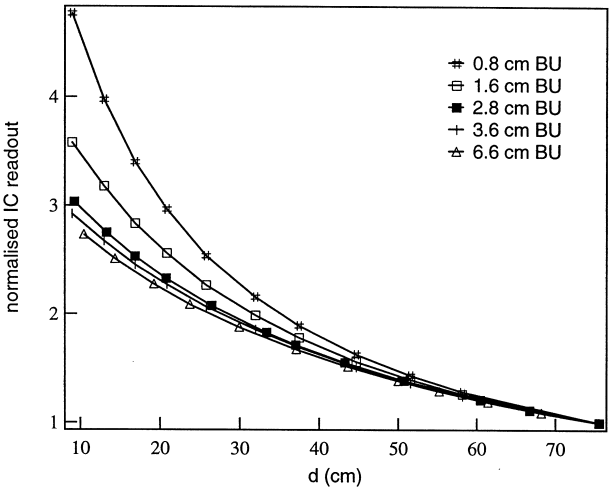

Fig. 3. Ion chamber measurements (as schematically illustrated in Fig. 1) in a mini-phantom under different build-up conditions as a function of the distance (d) between the exit surface of the multipurpose phantom and the ion chamber. All curves were normalised to their measuring point at an airgap of 75.5 cm.

When comparing images of the Las Vegas phantom obtained with and without build-up on the portal imager, no deterioration in image quality was observed for the images obtained with 1 or 2 cm polystyrene, or 1 mm copper.

3.3. Accuracy assessment of the EPID in dynamic mode

3.3.1. Relative dosimetry

The relative dosimetric accuracy of the dynamic acquisition mode is illustrated in Fig. 4, displaying a line profile extracted from the EPID dosimetric image to compare with the film scan (Fig. 4a) and the ion chamber measurements in a water phantom (Fig. 4b). All measurements were normalized on the beam-axis and show good agreement. Line profiles extracted from film and EPID measurements show an average deviation of 0.3%, with a SD of 1.9%. Comparable conclusions can be drawn from the data obtained with the ion chamber (average deviation of 0.7%; SD, 2.3%).

3.3.2. Data acquisition speed versus leaf speed

Fig. 5 shows two line scans extracted from the EPID images acquired during delivery of the dynamic leaf motion plan designed to produce blocks of leaves with constant leaf opening but different leaf speeds. Each block consisted of four adjacent leaves and line scans were extracted in the direction perpendicular to the leaf motion. The line scan obtained from the 400 MU delivery was theoretically rescaled to a 75 MU delivery by dividing the obtained signal through 5.33. This rescaled profile is in excellent relative agreement with the line scan extracted from the film (normalized to its maximum value), successively irradiated four times with the 75 MU delivery and also displayed in Fig. 5. The dosimetric EPID image of the 75 MU delivery, however, is of lesser quality (e.g. homogeneity of the dosimetric EPID image has deteriorated in regions that are homogeneous in the film measurement) and deviations amount to 26% for the lowest dose step (corresponding to the highest leaf speed, i.e. 3 cm/s).

3.3.3. Absolute dosimetry

The short-term absolute reproducibility was found to be excellent, i.e. ten dosimetric images of the same dynamic delivery, acquired within 1 day, agreed within 0.6% (1 SD). Images acquired over a span of several weeks lead to comparable results.

The linearity of the dose as a function of total amount of monitor units (MU_{tot}) is illustrated in Fig. 6. The absolute dose plotted in the figure is the integrated dose as measured

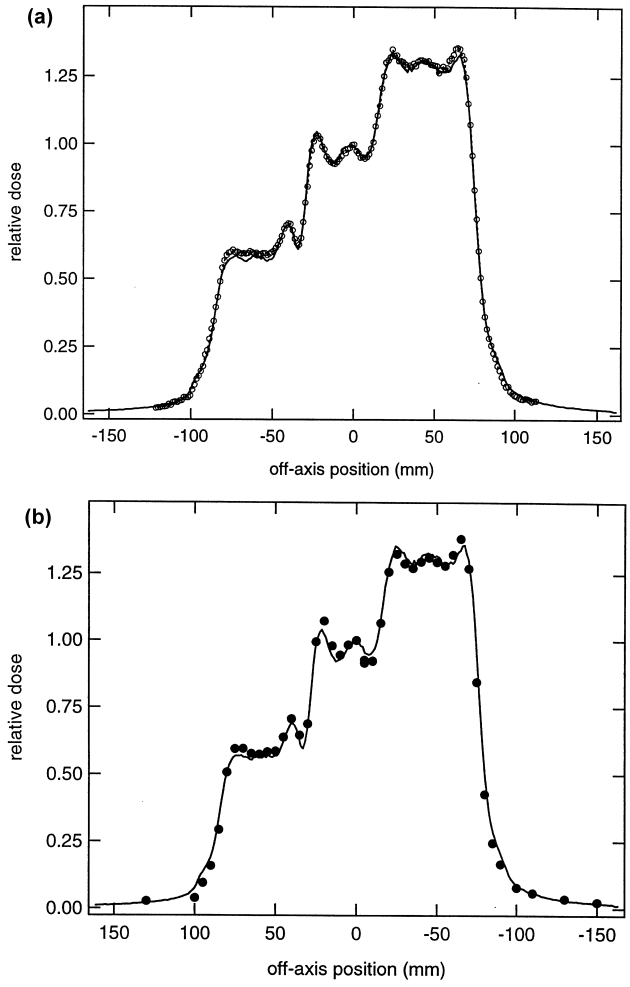

Fig. 4. Relative comparison of a line profile extracted from a dosimetric EPID image to: (a), a film scan (open symbols); and (b), ion chamber measurements in a water phantom (closed symbols). All measurements have been normalised to the data point on the beam-axis.

by the portal imager on the beam-axis during delivery of a dMLC plan with different MUs.

3.3.4. Calibration versus accelerator pulse rate frequency

Calibration of the dose–response relationship (Eq. (3)) for the dynamic acquisition mode performed for an 18 MV beam with dose rates of 100 and 200 MU/min, provided β values of 0.525 and 0.530, and α values of -2146 and -2190, respectively. Deviations from the calibration parameter values obtained at 300 MU/min ($\alpha = -2148$; $\beta = 0.545$) remained below 4%.

Fig. 7 displays dose profiles, all acquired with the calibration values for 300 MU/min, but with actual dose rates of 100, 200 and 300 MU/min. The largest deviations from delivery at 300 MU/min are observed for the data acquired at 100 MU/min (with a maximum deviation of 3%). Fig. 7 also displays the dose profile corresponding to the dynamic delivery with low leaf tolerance (0.05 mm). Dose rate adjustments were mainly present during movement of the

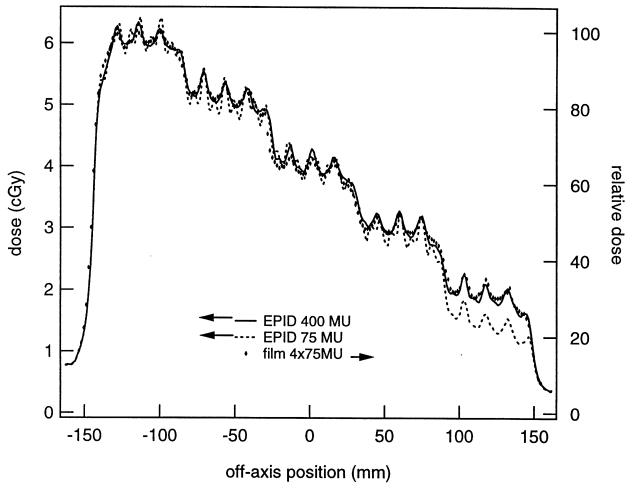

Fig. 5. Line scans extracted from dosimetric EPID images (left axis) acquired with 400 and 75 MU. The line scan from the 400 MU image was rescaled by division through 5.33. Data acquired from four-fold irradiation of a film and normalised to the maximum dose correspond to the right axis.

fastest leaf group where the dose rate fluctuated between 150 and 170 MU/min. Even so, the correspondence with the reference dosimetric image (tolerance, 0.2 mm) is better than 1%.

3.3.5. Memory effect of the EPID

Fig. 8 shows the theoretical and experimental decay of the ion concentration in the liquid after the beam has been switched off. Normalization to the initial ion concentration, i.e. the ion concentration at the moment of beam-off ($t = 0$), was performed by starting the image acquisition loop a few seconds before irradiation is stopped. The inset of Fig. 8 shows the remanence of a foregoing irradiation of a small 5×5 cm^2 field in an dosimetric image of a larger static field, taken as soon as physically possible (typically 20 s) after the

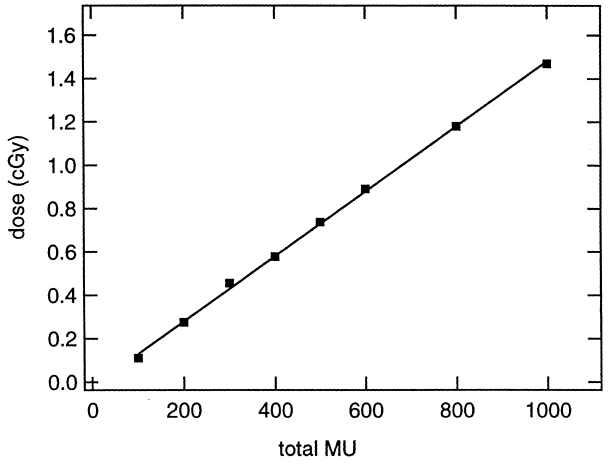

Fig. 6. Linearity of the integrated dose on the dosimetric EPID image as a function of the total amount of monitor units (MU_{tot}).

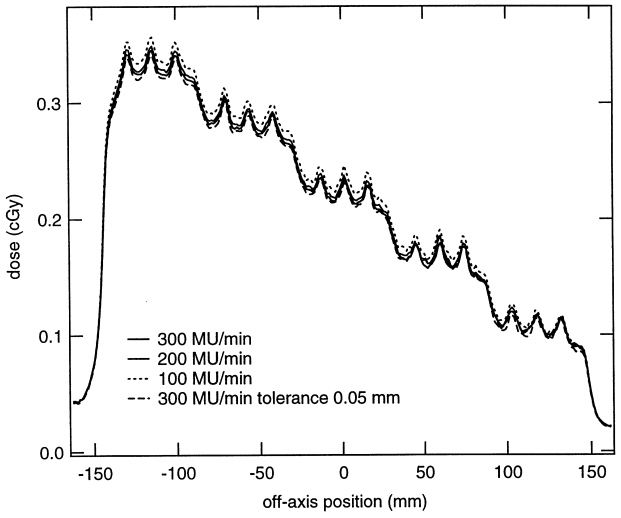

Fig. 7. EPID dose profiles acquired by 400 MU delivery of the same dMLC plan, but with different constant dose rates (100, 200 and 300 MU/min) and with fluctuating dose rates (tolerance, 0.05 mm). All images were converted to dose with the calibration values as determined with a dose rate of 300 MU/min. The line profile from the 300 MU/min irradiation is therefore the reference profile and printed in bold.

delivery of the small field. The profile has been normalized to the signal acquired 5 cm off-axis (i.e. outside of the area irradiated by the small field), illustrating the 2.5% contribution of the memory effect.

3.3.6. Image acquisition versus gantry angle

For each acquired verification flat field image, the gantry angle dependent correction as described by Eq. (6) was computed off-line. The result was compared with the images corrected with the standard correction scheme, i.e. without

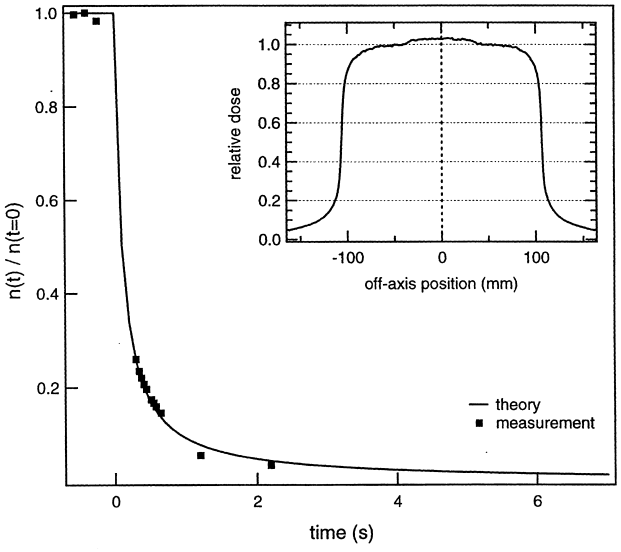

Fig. 8. Theoretical and experimental decay of the ion concentration in the liquid after irradiation has been terminated. The inset shows the remanence of a small static field irradiation foregoing the image acquisition of the larger static field.

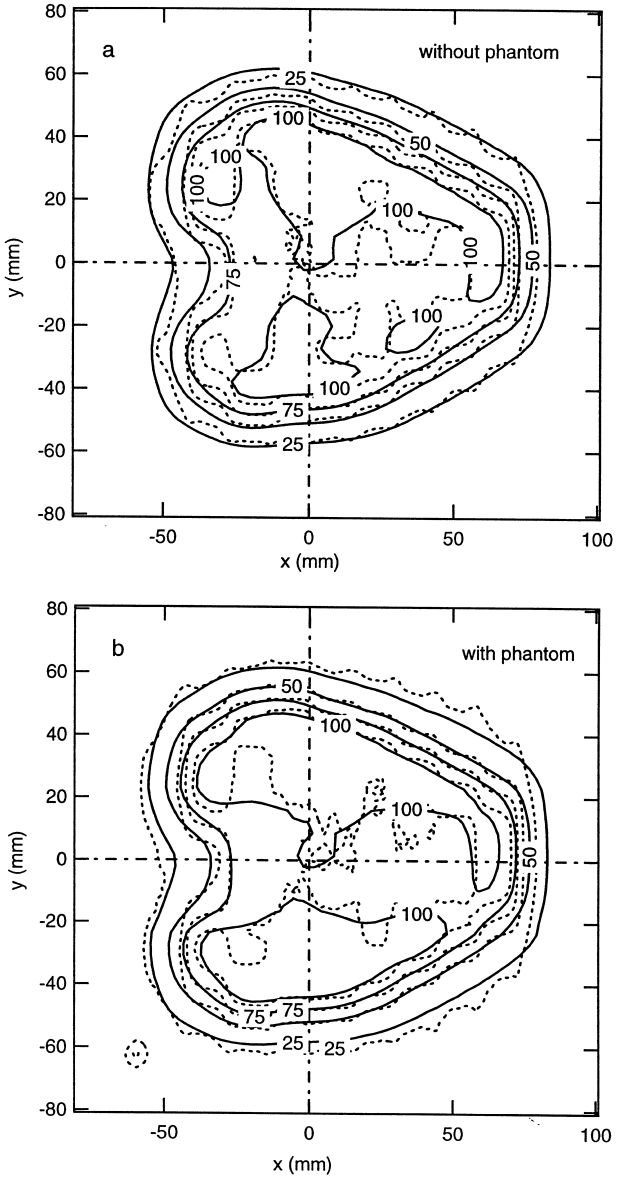

Fig. 9. Overlay of isodose lines for predicted (solid lines) and measured (dotted lines) dose distributions of an intensity modulated prostate field. Calculations and measurements have been performed: (a), without; and (b), with a heterogeneous rectangular phantom in the beam. All data have been normalised to the isocenter (i.e. 100% at $(x, y) = (0, 0)$).

taking the gantry angle into account. Images were converted to dose rate using the dose rate response function (Eq. (3)) to reflect the dosimetric error. The deviation from the expected value over the whole detector area, averaged over all gantry rotations (in steps of 10°), was reduced from 2.62 to 1.83% (1 SD); the maximum deviation decreased even more significantly.

3.4. Portal dose image prediction

Isodose lines of predicted and acquired dosimetric images of a prostate field are compared in Fig. 9. All images have been normalized to their value on the beam-axis (i.e. at

$(x, y) = (0, 0)$). Fig. 9a shows the results obtained without a patient or phantom in the beam: the overall agreement between both distributions is better than 3%, except at large dose gradients, where a slight positional mismatch between both images can introduce artificially large errors. Although not present in the predicted image, the MLC leaf pattern (e.g. interleaf leakage) can be distinguished in the measured isodose lines. The correspondence between predicted and EPID images is comparable when an inhomogeneous rectangular phantom is placed in the beam (Fig. 9b).

4. Discussion and conclusions

Accurate dosimetric images of intensity modulated beam profiles delivered with a dynamic multileaf collimator can be obtained with a commercially available, liquid-filled EPID (PortalVision Mk2, Varian). For this, a special acquisition mode had to be developed, allowing fast data acquisition (1.4 frames/s), unsynchronized to the accelerator pulses. The combination of both characteristics allows physical averaging over the ion concentration, making the measurement relatively insensitive to the accelerator pulse rate fluctuations.

When the EPID is used for dosimetry applications such as pre-treatment verification of the intensity modulated beams, sufficient build-up needs to be applied since the 8 mm water-equivalent build-up of the detector is insufficient to eliminate the contribution of scattered electrons to the dosimetric image. As these electrons are not taken into account in the used image prediction algorithm, an absence of build-up during measurement will generate large deviations between acquired and expected images, inhibiting both the relative and absolute evaluation of the dynamic delivery.

The relative accuracy of dosimetric images acquired under clinically relevant conditions (i.e. with leaf speed below 2 cm/s) shows excellent agreement with film measurements. Furthermore, two-dimensional dosimetry by means of the EPID is not limited to the narrow dosimetric range of conventional film measurements. Due to this limitation of film to an optimal dosimetric range, the non-ideal situation arises that planned treatment fields need to be delivered regularly with a different amount of MU for QA than during the actual delivery. Any error related to the leaf speed will therefore not be detected. The liquid-filled portal imager is not restricted to this limited dosimetric range, and most intensity modulated fields can be verified with the EPID under the exact conditions that will be used for treatment.

When the leaf speed is large compared with the data acquisition speed, i.e. when the number of acquired frames becomes insufficient to obtain a reliable average of the ion concentration, errors in the resulting dosimetric image become large, as illustrated in Fig. 5, where the leaf speed of the fastest leaf block reached 3.0 cm/s. Although the dosimetric image deteriorates both qualitatively and quantitatively, it must be stated that to obtain these high leaf speeds, the leaf position tolerance had to be increased from 0.2 mm, as used for clinical applications, to 0.5 mm. The maximum leaf speed observed with a tolerance of 0.2 mm was approximately 1.4 cm/s, corresponding to much smaller deviations from the reference dosimetric image.

Regarding absolute dosimetry, the measurements indicate a good short-term, as well as long-term, reproducibility. The linearity of the integrated dose as a function of the total amount of MU allows an easy workaround for pre-treatment verification of intensity modulated beams in rare cases where the clinical field parameters stretch the capabilities of the detector (extremely low amount of MU and/or high actual leaf speed). For pre-treatment quality control, such a clinical field can be delivered with a multiple of its original amount of MU and afterwards rescaled by simple division. The agreement between film (4×75 MU) and EPID measurements (75 and 400 MU) in Fig. 5 justifies this approach. However, when using this workaround, one must be aware of the fact that by increasing the amount of MU, errors related to the original leaf speed may go undetected.

The measurements as a function of accelerator pulse rate frequency show that even a permanent drop in the physical dose rate to 100 instead of 300 MU/min (at which calibration was performed) would still lead to dosimetric images of good relative and absolute accuracy. Artificially induced dose rate fluctuations during delivery of a single dynamic plan (Fig. 7) lead to a comparable conclusion: despite the fact that during movement of the fastest leaf groups the pulse rate dropped and fluctuated around 160 MU/min (instead of the prescribed and calibrated 300 MU/min), the correspondence with the reference dosimetric image (tolerance, 0.2 mm) is excellent.

In contrast to the findings of Curtin-Savard and Essers et al. [4,5], our measurements show that the ion concentration is reduced to 1% of its original value within a few seconds after irradiation has been terminated, indicating that remanence is small and clinically irrelevant in subsequent measurements of different treatment fields. Although still slightly visible in the inset of Fig. 8, the memory effect is small and would be even more negligible if the time between the two images was increased by a few seconds only, which will clearly be the case in the clinical routine, where the time to download the different dynamic MLC plans to the MLC workstation already suffices for the ion concentration to decay to less than 1% of its original value.

Bulging of the liquid film in the detector can be corrected for within 2–3% by a simple interpolation algorithm. When the correction is applied to the integrated image (at the external workstation), as made possible by the use of the power law dose–response relationship (Eq. (3)), the acquisition speed is left unchanged.

For the prostate fields displayed in Fig. 9, the average deviation between measured and calculated images is better

than 3%. Still, areas of larger deviations exist in between leaves and at steep dose gradients. The former is due to the fact that interleaf leakage is not taken into account by the TPS, and therefore, is not present in the expected fluence matrix on which the prediction is based. The latter discrepancy is merely the result of slight misalignments between calculation and prediction. In defining acceptance criteria for evaluating the measured dose distribution, a distinction should therefore be made between, for example, regions of high and low dose gradients; a technique for the quantitative evaluation of dose distributions making use of such a distinction is described by Low et al. [8].

An efficient procedure for pre-treatment verification of dynamic intensity modulated fields by means of the liquid-filled portal imager is realized by delivering the intensity modulated field to the portal imager without a patient or phantom in between. The acquired images are then compared with the image predictions. All measurements can be performed at a gantry angle of 0°, allowing not only faster, but also more accurate verification since bulging of the liquid need not be corrected for. Furthermore, it allows simple placement of a 2 cm build-up slab on the detector housing without the need for a more permanent fixation or mechanical adaptation of the detector. When all necessary tools for image comparison are available at the PortalVision workstation, a complete pre-treatment verification of all beams in a patient plan need not take more than 10–15 min. This presents a major advantage regarding the time required for patient specific quality assurance when compared with film measurements in a polystyrene phantom.

Verification of the intensity modulated beam profile during the actual delivery still remains of inferior accuracy. Although bulging of the liquid at non-zero gantry angles can not yet be entirely removed, the proposed correction algorithm is satisfactory, and accurate dosimetric images can be obtained at all gantry angles. The main difficulty in dosimetric verification during treatment remains the accurate prediction of the dosimetric reference image. The most important obstacles to deal with are: (i), the presence of the table and possible fixation devices, which can at present only be approximated by the prediction algorithm for a limited number of cases (gantry, 0, 90 and 270°); (ii), the absence of the build-up layer (unless one chooses to permanently mount the build-up into the portal imager so that it can be safely rotated around the patient); and (iii), variations in patient anatomy. Even so, the acquisition of a dosimetric image as presented in this work does not add much to the workload of the radiographers, and the day to day reproducibility of the dosimetry during treatment may be exploited to trace major discrepancies in patient set-up, patient anatomy or beam delivery.

Acknowledgements

During part of this work, A.V.E. was a senior research assistant of the IWT, Brussels (‘Vlaams Instituut voor de bevordering van het Wetenschappelijk-Technologisch onderzoek in de industrie). Part of this work was supported by a grant provided by Varian Medical Systems.

References

[1] Boellaard R, van Herk M, Mijnheer BJ. The dose–response relationship of a liquid-filled electronic portal imaging device. Med Phys 1996;23:1601–1611.
[2] Burman C, Chui C, Kutcher G, et al. Planning, delivery and quality assurance of intensity modulated radiotherapy using dynamic multileaf collimator: a strategy for large-scale implementation for the treatment of carcinoma of the prostate. Int J Radiat Oncol Biol Phys 1997;39:863–873.
[3] Chang J, Mageras GS, Chui C, Ling CC, Lutz W. Relative profile and dose verification of intensity-modulated radiation therapy. Int J Radiat Oncol Biol Phys 2000;47(1):231–240.
[4] Curtin-Savard AJ, Podgorsak EB. Verification of segmented beam delivery using a commercial electronic portal imaging device. Med Phys 1999;26(5):737–742.
[5] Essers M, Hoogervorst BR, van Herk M, Lanson H, Mijnheer BJ. Dosimetric characteristics of a liquid-filled electronic portal imaging device. Int J Radiat Oncol Biol Phys 1995;33(5):1265–1272.
[6] James HV, Atherton S, Budgell GJ, Kirby MC, Williams PC. Verification of dynamic multileaf collimation using an electronic portal imaging device. Phys Med Biol 2000;45:495–509.
[7] LoSasso T, Chui C, Ling CC. Physical and dosimetric aspects of a multileaf collimation system used in the dynamic mode for implementing intensity modulated radiotherapy. Med Phys 1998;25:1919–1927.
[8] Low DA, Harms WB, Mutic S, Purdy JA. A technique for the quantitative evaluation of dose distributions. Med Phys 1998;25(5):656–661.
[9] Ma L, Geis PB, Boyer L. Quality assurance for dynamic multileaf collimator modulated fields using a fast beam imaging system. Med Phys 1997;24(8):1213–1220.
[10] Mohan R, Wang X, Jackson A, et al. The potential and limitations of the inverse radiotherapy technique. Radiother Oncol 1994;32:232–248.
[11] Pasma KL, Heijmen BJM, Kroonwijk M, Visser AG. Portal dose image prediction for dosimetric treatment verification in radiotherapy: an algorithm for open beams. Med Phys 1998;25(6):830–840.
[12] Pasma KL, Dirkx MLP, Kroonwijk M, Visser AG, Heijmen BJM. Dosimetric verification of intensity modulated beams produced with dynamic multileaf collimation using an electronic portal imaging device. Med Phys 1999;26(11):2373–2378.
[13] Storchi P, Woudstra E. Calculation models for determining the absorbed dose in water phantoms in off-axis planes of rectangular fields of open and wedged photon beams. Phys Med Biol 1995;40:511–527.
[14] Storchi P, Woudstra E. Calculation or the absorbed dose distribution due to irregularly shaped photon beams using pencil beam kernels derived from basic input data. Phys Med Biol 1996;41:637–656.
[15] Stucchi P, Conte L, Mordacchini C, et al. The use of an electronic portal imaging device for exit dosimetry. Abstract 75. Third Biennial Meeting of the European Society for Therapeutic Radiology and Oncology, Gardona Riviera, Italy, 1995.
[16] van Herk M. Physical aspects of a liquid-filled ionization chamber with pulsed polarizing voltage. Med Phys 1991;18:692–702.
[17] Wang X, Spiridon S, LoSasso T, Stein J, Chui C, Mohan R. Dosimetric verification of intensity modulated fields. Med Phys 1996;23:317–327.